A Nonlinear Motion Cueing Algorithm with a Human Perception Model

Robert J. Telban

Department of Mechanical Engineering

State University of New York at Binghamton

Binghamton, NY 13902-6000

Research Advisor: Professor Frank Cardullo

ABSTRACT

This paper describes new developments in motion cueing algorithms for the control of flight simulator motion systems. The research discussed is being conducted in four phases: linear motion cueing algorithm development, vestibular and human perceptual system modeling, nonlinear cueing algorithm development, and cueing algorithm performance testing.

A variation of the so-called optimal algorithm was formulated using simulated aircraft angular velocity input as a basis. Models of the human vestibular sensation system, i.e. the semicircular canals and otoliths, are incorporated within the algorithm. Results compared favorably with the coordinated adaptive washout algorithm, yielding similar results for angular velocity cues while eliminating false cues and reducing the tilt rate for longitudinal cues.

Literature studies in motion sensation and the vestibular system have been conducted to develop vestibular system sensation models that are most consistent with both experimental and theoretical analyses. Improved models of both the semicircular canals and the otoliths are proposed. Literature studies of the characteristics of visually induced motion sensation and the visual-vestibular interaction have also been conducted. An integrated human perception model is proposed that includes both visual and vestibular sensation and incorporates the interaction between the stimuli. The addition of the optokinetic influence in the linear algorithm was shown to improve the response to a surge input, producing a specific force response with no steady-state washout and a further decrease in the tilt rate.

A novel approach to motion cueing is proposed, combining features of the adaptive and optimal algorithms, and incorporating the improved vestibular models and the proposed integrated motion perception model. The algorithm is formulated as an optimal control problem with a nonlinear control law. The control law requires the matrix Riccati equation to be solved in real time; a neurocomputing approach is used to solve this computationally challenging problem. Results for the yaw mode reveal that the nonlinear algorithm improves the motion cues by reducing the magnitude of negative cues. The heave mode responses show a reduction in the peak onset displacement command that, when scaling the response within the motion platform limits, will yield an increased onset cue.

The effectiveness of the nonlinear algorithm as compared to the adaptive and linear optimal algorithms will be evaluated on a motion platform with a series of pilot controlled maneuvers. The results of this evaluation will be used to assess motion cueing algorithm performance.

INTRODUCTION

The objective of a motion system, when used in conjunction with a visual system, is to stimulate the pilot so that he can perceive the required motion cues necessary to fly the simulator within the same performance and control activity as the aircraft. An example of a motion system is the six-degree-of-freedom hexapod shown in Figure 1.

Figure 1. Six-Degree-of-Freedom Hexapod Motion System.

Simulator motion allows the pilot to react more quickly to simulated aircraft dynamics as compared to visual stimuli alone, thus enabling him to correct (and reduce the magnitude) of any deviation sooner than having to wait for the information visually. Studies have been reported that support motion improving pilot performance [1], [2], [3], [4].

The vehicle simulation structure for a motion system is shown in Figure 2. The operator control inputs drive a mathematical model of the vehicle dynamics, generating the vehicle states. The desired motion cues and motion platform states are produced by passing the vehicle states through the motion cueing algorithm. The desired motion platform states are then transformed from degree-of-freedom space to actuator space, generating the desired commands to the six actuators. The actuator motion commands serve as input to the closed-loop platform dynamics, resulting in actual simulator motion.

The motion cueing algorithm generates the desired motion cues that are constrained within the physical limits of the motion system. The magnitude of the cues is reduced by scaling and limiting the vehicle states. The duration of the cues is limited by a technique known as washout. Washout involves returning the motion platform states to a neutral position following the initial, or "onset" portion of a motion cue, thus "washing out" the resulting cue at levels below the pilot's perceptual threshold. This is accomplished by passing the vehicle state through a high-pass filter, removing long-duration (low-

frequency) motion components. Early approaches to washout filtering used simple (first- and second-order) linear filters in which the ratio of onset to washout duration was fixed. Nonlinear approaches were later developed where this ratio varied with time.

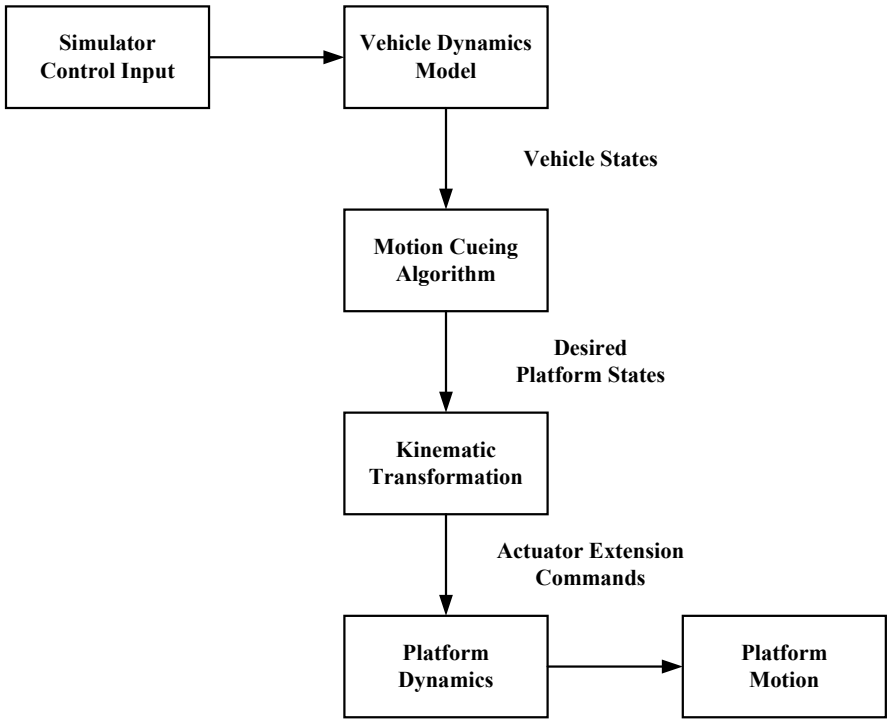

Figure 2. Vehicle Simulation Structure for a Motion System.

The otolith organs in the human vestibular system sense both acceleration and tilting of the pilot's head with respect to the gravity vector. Since the otoliths cannot discriminate between acceleration and tilt, this phenomenon, known as tilt coordination, can be used to advantage in motion simulation. For long-term specific force simulation, acceleration cues simulated by high-pass washout filters are augmented by tilting the motion platform at a rate below the pilot's perceptual threshold. This additional cue results from passing the vehicle acceleration through a low-pass filter to produce the desired long-duration tilt cue. Tilt coordination is implemented in a motion cueing algorithm by adding additional filters in the longitudinal (pitch/surge) and lateral (roll/sway) modes that produce the additional cues. For this reason four separate modes are implemented in a motion cueing algorithm: longitudinal, lateral, yaw, and heave.

Two viable approaches to motion cueing were identified from research conducted by Wu and Cardullo [5]. The first technique is a modification of the coordinated adaptive washout algorithm, or "adaptive algorithm" developed at NASA by Parrish, et al. [6]. The objective of this algorithm is to adjust the motion platform response based upon its current motion states by minimizing a cost function in real time. The cost function is minimized by continuously adjusting a set of adaptive parameters by the method of steepest descent. This technique has at its basis the minimization of state error between the aircraft and simulator.

The second technique is the "optimal algorithm", based on that which was first developed by Sivan, et al. [7], and later implemented by Reid and Nahon [8]. This algorithm uses higher order linear filters that are developed, prior to real time implementation, using optimal control methods. This method incorporates a mathematical model of the human vestibular system, constraining the pilot sensation error between the simulated aircraft and motion platform dynamics. An improved development of this algorithm is discussed in further detail in the next section.

In this research a novel approach to motion cueing is proposed that combines features of the adaptive and optimal algorithms. This algorithm incorporates human vestibular models along with a proposed integrated human perception model. The algorithm is formulated as an optimal control problem with a nonlinear control law, resulting in a set of nonlinear cueing filters that are adjusted in real time based on the motion platform and perceptual error states. A neurocomputing approach to solve the matrix Riccati equation in real time is discussed. Preliminary results for this proposed algorithm are presented.

The effectiveness of the proposed algorithm as compared to the adaptive and linear optimal algorithms will be evaluated on a motion platform with a series of pilot controlled maneuvers. A description of the proposed methods of evaluation is given.

LINEAR OPTIMAL MOTION CUEING ALGORITHM

Problem Description

In developing a set of optimal washout filters, the problem is to determine a matrix of transfer functions **W(s)** that relate the desired simulator motion input to the aircraft input such that a cost function constraining the pilot sensation error (between simulator and aircraft) is minimized. The structure of this problem is illustrated in Figure 3.

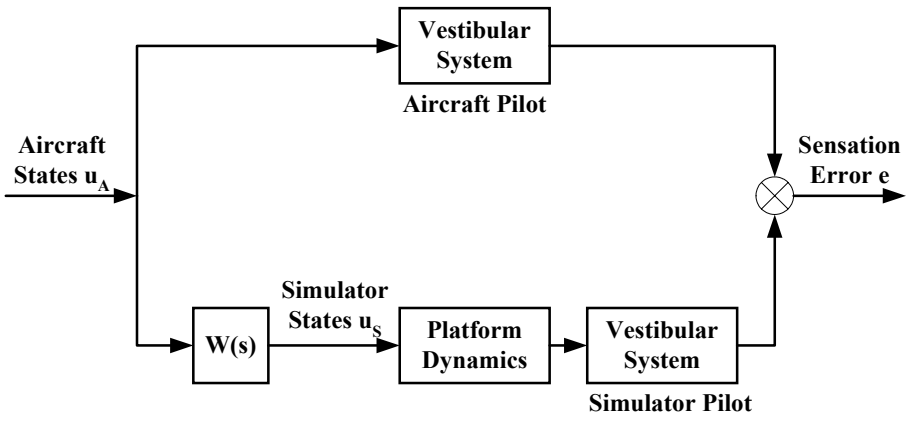

Figure 3. Optimal Algorithm Problem Structure.

A mathematical model of the human vestibular system is used in the filter development. The optimal algorithm generates the desired transfer functions **W(s)** by an off-line program, which are then implemented on-line. **W(s)** will relate the simulator

motion states to the aircraft states by $\mathbf{u_S} = \mathbf{W(s)} \times \mathbf{u_A}$. The simulator states $\mathbf{u_S}$ are then used to generate the desired motion platform commands.

In the original development the washout filters were applied in the pilot head reference frame. Reid and Nahon [8] noted that this frame selection was chosen to eliminate sensation cross-couplings that made the development of **W(s)** more complicated. Wu [9] demonstrated that this location of the center of rotation at the pilot's head resulted in excessively large actuator extensions in some input cases. He suggested that the optimal algorithm be reformulated in the simulator reference frame with the center of rotation located at the centroid of the simulator motion-base.

The question has arisen as to what aircraft and simulator control inputs are the most appropriate for the optimal algorithm. The previous developments [7], [8] suggested a control input for either the longitudinal or lateral mode with linear acceleration and angular displacement as control inputs. Wu [9] developed an approach using linear acceleration and angular acceleration for the longitudinal mode. This approach showed advantages in controlling additional modes that were not available in the original development. In addition, since the semicircular canals behave as a transducer for angular velocity input in the range of normal head movements, an approach using angular velocity as input is desired. In this research an optimal algorithm based on simulated aircraft angular velocity inputs is developed.

Linear Optimal Algorithm Development

The algorithm development with angular velocity input for the longitudinal (pitch/surge) mode is given below. The input **u** is formulated as

$$\mathbf{u} = \begin{bmatrix} \dot{\theta} \\ a_x \end{bmatrix} = \begin{bmatrix} u_1 \\ u_2 \end{bmatrix}, \tag{1}$$

where $\dot{\theta}$ is angular velocity, and a_x is the translational acceleration, with each term respectively set equal to u_1 and u_2. The sensed rotational motion $\hat{q}$ is then related to the input **u** by

$$\begin{aligned} \dot{\mathbf{x}}_{\mathbf{1\sim3}} &= \mathbf{A_{SCC}}\mathbf{x_{1\sim3}} + \mathbf{B_{SCC}}\mathbf{u}\,, \\ \hat{q} &= \mathbf{C_{SCC}}\mathbf{x}_{1\sim3} + \mathbf{D_{SCC}}\mathbf{u}\,, \end{aligned} \tag{2}$$

where $\mathbf{x_{1\sim3}}$ are the semicircular canals states, and $\mathbf{A_{SCC}}$, $\mathbf{B_{SCC}}$, $\mathbf{C_{SCC}}$, and $\mathbf{D_{SCC}}$ represent the semicircular canals model in state space. The sensed specific force $\hat{f}_x$ is then related to the input **u** by

$$\begin{aligned} \dot{\mathbf{x}}_{\mathbf{4\sim8}} &= \mathbf{A_{OTO}}\mathbf{x_{4\sim8}} + \mathbf{B_{OTO}}\mathbf{u}\,, \\ \hat{f}_x &= \mathbf{C_{OTO}}\mathbf{x_{4\sim8}} + \mathbf{D_{OTO}}\mathbf{u}\,, \end{aligned} \tag{3}$$

where $\mathbf{x_{4\sim8}}$ are the otoliths states, and $\mathbf{A_{OTO}}$, $\mathbf{B_{OTO}}$, $\mathbf{C_{OTO}}$, and $\mathbf{D_{OTO}}$ represent the otoliths model in state space. The transfer function representations for these models are discussed

in the next section. The representations in Eqns. (2) and (3) can be combined to form a single representation for the human vestibular model:

$$\begin{aligned} \dot{\mathbf{x}}_{1\sim 8} &= \mathbf{A}_V \mathbf{x}_{1\sim 8} + \mathbf{B}_V \mathbf{u} \,, \\ \hat{\mathbf{y}}_1 &= \mathbf{C}_V \mathbf{x}_{1\sim 8} + \mathbf{D}_V \mathbf{u} \,, \end{aligned} \tag{4}$$

where $\mathbf{x}_{1\sim 8}$ and $\hat{\mathbf{y}}_1$ are, respectively, the combined states and sensed responses, and $\mathbf{A}_V$, $\mathbf{B}_V$, $\mathbf{C}_V$, and $\mathbf{D}_V$ represent the vestibular models as one set of state equations:

$$\mathbf{A}_V = \begin{bmatrix} \mathbf{A}_{SCC} & \mathbf{0} \\ \mathbf{0} & \mathbf{A}_{OTO} \end{bmatrix}, \quad \mathbf{B}_V = \begin{bmatrix} \mathbf{B}_{SCC} \\ \mathbf{B}_{OTO} \end{bmatrix}, \quad \mathbf{C}_V = \begin{bmatrix} \mathbf{C}_{SCC} & \mathbf{0} \\ \mathbf{0} & \mathbf{C}_{OTO} \end{bmatrix}, \quad \mathbf{D}_V = \begin{bmatrix} \mathbf{D}_{SCC} \\ \mathbf{D}_{OTO} \end{bmatrix}.$$

It is assumed that the same sensation model can be applied to both the pilot in the aircraft and the pilot in the simulator as shown in Figure 3. We then define the vestibular state error $\mathbf{x}_e = \mathbf{x}_S - \mathbf{x}_A$ (where $\mathbf{x}_S$ and $\mathbf{x}_A$ are the respective vestibular states for the simulator and aircraft), and the pilot sensation error $\mathbf{e}$, resulting in

$$\begin{aligned} \dot{\mathbf{x}}_e &= \mathbf{A}_V \mathbf{x}_e + \mathbf{B}_V \mathbf{u}_S - \mathbf{B}_V \mathbf{u}_A \,, \\ \mathbf{e} &= \mathbf{C}_V \mathbf{x}_e + \mathbf{D}_V \mathbf{u}_S - \mathbf{D}_V \mathbf{u}_A \,, \end{aligned} \tag{5}$$

where $\mathbf{u}_S$ and $\mathbf{u}_A$ represent the simulator and aircraft inputs as given in Eqn. (1).

It is also necessary for the control algorithm to explicitly access motion states such as the linear velocity and displacement of the motion platform, which are desired to appear in the cost function. For this purpose additional terms are included in the state equations:

$$\dot{\mathbf{x}}_d = \mathbf{A}_d \mathbf{x}_d + \mathbf{B}_d \mathbf{u}_S \,, \tag{6}$$

where $\mathbf{x}_d$ represents the additional motion platform states:

$$\mathbf{x}_d = \begin{bmatrix} \iiint a_x dt^3 & \iint a_x dt^2 & \int a_x dt & \theta \end{bmatrix}^T,$$

and are related to the simulator input $\mathbf{u}_S$ by

$$\mathbf{A}_d = \begin{bmatrix} 0 & 1 & 0 & 0 \\ 0 & 0 & 1 & 0 \\ 0 & 0 & 0 & 0 \\ 0 & 0 & 0 & 0 \end{bmatrix}, \quad \mathbf{B}_d = \begin{bmatrix} 0 & 0 \\ 0 & 0 \\ 0 & 1 \\ 1 & 0 \end{bmatrix}.$$

The aircraft input $\mathbf{u}_A$ consists of filtered white noise, and can be expressed as

$$\begin{aligned} \dot{\mathbf{x}}_\mathbf{n} &= \mathbf{A}_\mathbf{n}\mathbf{x}_\mathbf{n} + \mathbf{B}_\mathbf{n}\mathbf{w}\,, \\ \mathbf{u}_\mathbf{A} &= \mathbf{x}_\mathbf{n}\,, \end{aligned} \tag{7}$$

where $\mathbf{x_n}$ are the filtered white noise states, $\mathbf{w}$ represents white noise, with $\mathbf{A_n}$ and $\mathbf{B_n}$ given as

$$\mathbf{A_n} = \begin{bmatrix} -\omega_1 & 0 \\ 0 & -\omega_2 \end{bmatrix}, \quad \mathbf{B_n} = \begin{bmatrix} \omega_1 \\ \omega_2 \end{bmatrix},$$

where ω_1 and ω_2 are the first-order filter break frequencies for each degree-of-freedom. The state equations given in Eqns. (5), (6), and (7) can be combined to form the desired system equation

$$\begin{aligned} \dot{\mathbf{x}} &= \mathbf{A}\mathbf{x} + \mathbf{B}\mathbf{u}_\mathbf{S} + \mathbf{H}\mathbf{w}\,, \\ \mathbf{y} &= \begin{bmatrix} \mathbf{e} & \mathbf{x_d} \end{bmatrix}^\mathbf{T} = \mathbf{C}\mathbf{x} + \mathbf{D}\mathbf{u}_\mathbf{S}\,, \end{aligned} \tag{8}$$

where $\mathbf{y}$ is the desired output, and $\mathbf{x} = \begin{bmatrix} \mathbf{x_e} & \mathbf{x_d} & \mathbf{x_n} \end{bmatrix}^\mathbf{T}$ represents the combined states. The combined system matrices $\mathbf{A}$, $\mathbf{B}$, $\mathbf{C}$, $\mathbf{D}$, and $\mathbf{H}$ are then given by

$$\mathbf{A} = \begin{bmatrix} \mathbf{A_V} & \mathbf{0} & \mathbf{-B_V} \\ \mathbf{0} & \mathbf{A_d} & \mathbf{0} \\ \mathbf{0} & \mathbf{0} & \mathbf{A_n} \end{bmatrix}, \quad \mathbf{B} = \begin{bmatrix} \mathbf{B_V} \\ \mathbf{B_d} \\ \mathbf{0} \end{bmatrix}, \quad \mathbf{H} = \begin{bmatrix} \mathbf{0} \\ \mathbf{0} \\ \mathbf{B_n} \end{bmatrix},$$
$$\mathbf{C} = \begin{bmatrix} \mathbf{C_V} & \mathbf{0} & \mathbf{-D_V} \\ \mathbf{0} & \mathbf{I} & \mathbf{0} \end{bmatrix}, \quad \mathbf{D} = \begin{bmatrix} \mathbf{D_V} \\ \mathbf{0} \end{bmatrix}.$$

A cost function J is then defined as

$$J = E\left\{ \int_{t_0}^{t_1} \left(\mathbf{e}^\mathbf{T}\mathbf{Q}\mathbf{e} + \mathbf{x}_\mathbf{d}^\mathbf{T}\mathbf{R_d}\mathbf{x_d} + \mathbf{u}_\mathbf{S}^\mathbf{T}\mathbf{R}\,\mathbf{u}_\mathbf{S} \right) dt \right\}, \tag{9}$$

where $E\{\ \}$ is the mathematical mean of statistical variable, $\mathbf{Q}$ and $\mathbf{R_d}$ are positive semi-definite matrices, and $\mathbf{R}$ is a positive definite matrix. Eqn. (9) implies that three variables are to be constrained in the cost function: the sensation error $\mathbf{e}$ along with the additional terms $\mathbf{x_d}$ and $\mathbf{u_S}$ which together define the linear and angular motion of the platform. The cost function constrains both the sensation error and the platform motion.

The system equation and cost function can be transformed to the standard optimal control form as shown in Kwakernaak and Sivan [10] and noted in Reid and Nahon [8] by the following equations:

$$\dot{\mathbf{x}} = \mathbf{A}'\mathbf{x} + \mathbf{B}\mathbf{u}' + \mathbf{H}\mathbf{w}\,,$$
$$J' = E\left\{\int_{t_0}^{t_1}\left(\mathbf{x}^{\mathrm{T}}\mathbf{R}_1'\mathbf{x} + \mathbf{u}'^{\mathrm{T}}\mathbf{R}_2\mathbf{u}'\right)dt\right\}, \tag{10}$$

where

$$\mathbf{A}' = \mathbf{A} - \mathbf{B}\mathbf{R}_2^{-1}\mathbf{R}_{12}^{\mathrm{T}}\,,\quad \mathbf{u}' = \mathbf{u}_{\mathrm{S}} + \mathbf{R}_2^{-1}\mathbf{R}_{12}^{\mathrm{T}}\mathbf{x}\,,\quad \mathbf{R}_1' = \mathbf{R}_1 - \mathbf{R}_{12}\mathbf{R}_2^{-1}\mathbf{R}_{12}^{\mathrm{T}}\,,$$
$$\mathbf{R}_1 = \mathbf{C}^{\mathrm{T}}\mathbf{G}\mathbf{C}\,,\quad \mathbf{R}_{12} = \mathbf{C}^{\mathrm{T}}\mathbf{G}\mathbf{D}\,,\quad \mathbf{R}_2 = \mathbf{R} + \mathbf{D}^{\mathrm{T}}\mathbf{G}\mathbf{D}\,,\quad \mathbf{G} = \begin{bmatrix}\mathbf{Q} & \mathbf{0}\\ \mathbf{0} & \mathbf{R}_{\mathrm{d}}\end{bmatrix}.$$

The cost function of Eqn. (10) is minimized when

$$\mathbf{u}_{\mathrm{S}} = -\left[\mathbf{R}_2^{-1}\left(\mathbf{B}^{\mathrm{T}}\mathbf{P} + \mathbf{R}_{12}^{\mathrm{T}}\right)\right]\mathbf{x}\,, \tag{11}$$

where $\mathbf{P}$ is the solution of the algebraic Riccati equation

$$\mathbf{R}_1' - \mathbf{P}\mathbf{B}\mathbf{R}_2^{-1}\mathbf{B}^{\mathrm{T}}\mathbf{P} + \mathbf{A}'^{\mathrm{T}}\mathbf{P} + \mathbf{P}\mathbf{A}' = \mathbf{0}\,, \tag{12}$$

Defining a matrix $\mathbf{K}$, where $\mathbf{u}_{\mathrm{S}} = \mathbf{K}\mathbf{x}$,

$$\mathbf{K} = \mathbf{R}_2^{-1}\left(\mathbf{B}^{\mathrm{T}}\mathbf{P} + \mathbf{R}_{12}^{\mathrm{T}}\right), \tag{13}$$

$\mathbf{K}$ can be partitioned corresponding to the partition of $\mathbf{x}$ in Eqn. (8):

$$\mathbf{u}_{\mathrm{S}} = -\begin{bmatrix}\mathbf{K}_1 & \mathbf{K}_2 & \mathbf{K}_3\end{bmatrix}\begin{bmatrix}\mathbf{x}_{\mathrm{e}}\\ \mathbf{x}_{\mathrm{d}}\\ \mathbf{x}_{\mathrm{n}}\end{bmatrix} + \begin{bmatrix}\mathbf{B}_{\mathrm{V}}\\ \mathbf{B}_{\mathrm{d}}\end{bmatrix}\mathbf{u}_{\mathrm{S}}\,. \tag{14}$$

Noting that $\mathbf{x}_{\mathrm{n}} = \mathbf{u}_{\mathrm{A}}$, remove the states corresponding to the $\mathbf{x}_{\mathrm{n}}$ partition from Eqn. (14):

$$\begin{bmatrix}\dot{\mathbf{x}}_{\mathrm{e}}\\ \dot{\mathbf{x}}_{\mathrm{d}}\end{bmatrix} = \begin{bmatrix}\mathbf{A}_{\mathrm{V}} & \mathbf{0} & -\mathbf{B}_{\mathrm{V}}\\ \mathbf{0} & \mathbf{A}_{\mathrm{d}} & \mathbf{0}\end{bmatrix}\begin{bmatrix}\mathbf{x}_{\mathrm{e}}\\ \mathbf{x}_{\mathrm{d}}\\ \mathbf{u}_{\mathrm{A}}\end{bmatrix} + \begin{bmatrix}\mathbf{B}_{\mathrm{V}}\\ \mathbf{B}_{\mathrm{d}}\end{bmatrix}\mathbf{u}_{\mathrm{S}}\,. \tag{15}$$

After taking the Laplace transform of Eqns. (14) and (15), the following equations are obtained in the Laplace domain:

$$\mathbf{u}_{\mathrm{S}}(\mathbf{s}) = \mathbf{W}(\mathbf{s}) \times \mathbf{u}_{\mathrm{A}}(\mathbf{s})\,, \tag{16}$$

where $\mathbf{W(s)} = \begin{bmatrix} \mathbf{K_1} & \mathbf{K_2} \end{bmatrix} \begin{bmatrix} \mathbf{sI - A_V + B_V K_1} & \mathbf{B_V K_2} \\ \mathbf{B_d K_1} & \mathbf{sI - A_d + B_d K_2} \end{bmatrix}^{-1} \begin{bmatrix} \mathbf{B_V (I + K_3)} \\ \mathbf{B_d K_3} \end{bmatrix} - \mathbf{K_3}$.

The optimal filter matrix **W(s)** is computed using a set of MATLAB scripts. The weighting matrices **Q**, **R**, and $\mathbf{R_d}$ given in the cost function of Eqn. (9) are selected and adjusted to produce the desired motion platform commands. From these weights and the vestibular models the standard optimal control matrices of Eqn. (10) are computed. The algebraic Riccati equation of Eqn. (12) is solved with the MATLAB function **"care"**. The solution for **W(s)** is then computed. Common poles and zeros are cancelled in each transfer function, yielding a set of seventh-order filters for the longitudinal mode. These filters are then used in a SIMULINK model that generates the linear acceleration and angular velocity responses. Similar developments will yield filters for the lateral, yaw, and heave modes.

Prior to input to the transfer matrix **W(s)**, the aircraft inputs $\mathbf{u_A}$ are transformed from the simulator reference frame to the inertial reference frame, and are then scaled with a nonlinear gain algorithm proposed by Wu [9]. The simulator inputs $\mathbf{u_S}$ are integrated to produce the desired motion-base displacement commands that are then used to compute the desired actuator commands as noted in Figure 2.

Linear Algorithm Evaluation

Comparisons of longitudinal degree-of-freedom commands are made between the optimal algorithm with angular velocity input and the adaptive algorithm. Test runs are generated with single degree-of-freedom aircraft inputs. The translational break frequency as given in Eqn. (15) was increased from 1 rad/s to 4π rad/s in both algorithms to minimize an onset false cue for responses to a surge step input. Comparisons are made of specific force at the pilot's head and platform angular velocity, as well as responses filtered through vestibular system models.

The specific force responses to a ramp to step surge input of magnitude 1 m/s^2 and slope 3 $m/s^2/s$ are shown in Figure 4. The adaptive algorithm produces a significant false cue (-0.5 m/s^2) at onset, after which the peak is followed by a "sag" (decrease followed by increase) for about 5 seconds until a steady magnitude is reached. The optimal algorithm produces no false cue with a smooth ramp at onset followed by a smaller peak magnitude and faster washout. The sensed specific force responses show the simulator pilot response from the optimal algorithm, while reduced in magnitude, closely tracks the shape of the sensed response of the aircraft pilot. The adaptive algorithm does not track the shape of the aircraft pilot sensed response as well, especially for the duration where the sag occurred.

Angular velocity (pitch) responses due to tilt coordination generated by the surge cue are shown in Figure 5. The responses show a lower peak velocity at onset for the optimal algorithm by about 1 deg/s but followed by a negative peak of about 1 deg/s before the platform settles to zero velocity. The adaptive algorithm settles to zero velocity with no negative peak.

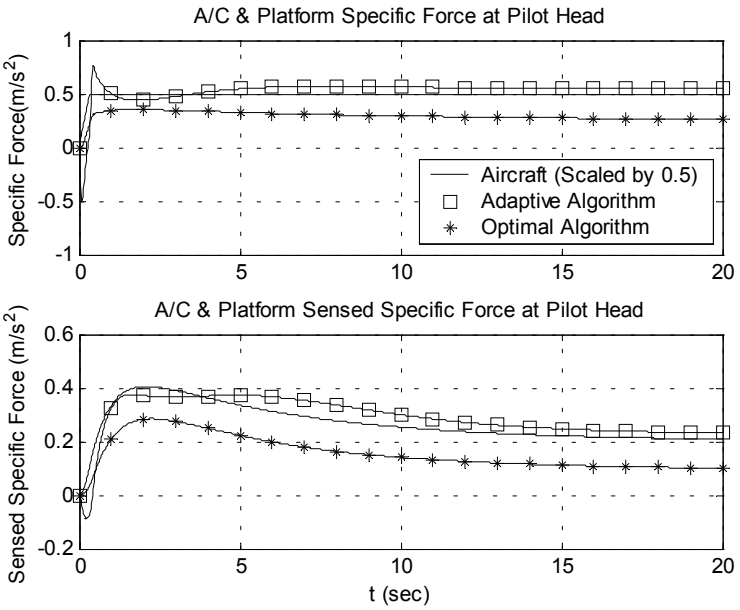

Figure 4. Comparison of Adaptive and Optimal Algorithm Responses for Aircraft Surge Input.

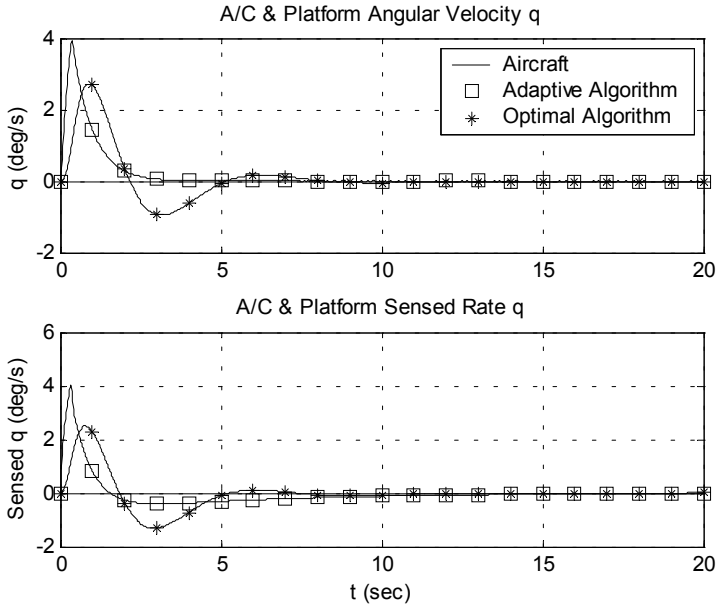

Figure 5. Platform Tilt Coordination Commands for Aircraft Surge Input.

Angular velocity responses to a pitch acceleration doublet input show that the optimal and adaptive algorithm responses are nearly identical; each response is a proportionately reduced magnitude of the aircraft angular velocity input. The specific force response in the z-axis due to the pitch cue is smaller in magnitude (and closer to the aircraft response) for the optimal algorithm as compared to the adaptive algorithm response; this is consistent with the slightly larger pitch cue that results for the optimal algorithm [11].

VESTIBULAR SYSTEM MODELING

Semicircular Canals Model

Zacharias [12] reported that a linear second-order model of the semicircular canals was first developed to explain the observed characteristics of vestibular induced eye movements in fish (pike). This model was further refined by the "torsion-pendulum" model of Van Egmond, et al. [13], and is later developed from a systems approach by Mayne [14]. The transfer function for this overdamped system is

$$\frac{\theta_e(s)}{\alpha(s)} = \frac{\tau_1\tau_2}{(1+\tau_1 s)(1+\tau_2 s)}, \tag{17}$$

where α is the angular acceleration of the head with respect to an inertial axis, θ_e is the angular displacement of the endolymph with respect to the head, and τ_1 and τ_2 are time constants, with $\tau_1 >> \tau_2$. Schmid, et al. [15], showed that θ_e and the cupula deflection ϕ_c are related by $\phi_c = -a\theta_e$, where a is a constant.

Further studies showed that rotational sensation is more complex than the torsion-pendulum model. Young and Oman [16] formulated an adaptation operator and cascaded it with the torsion-pendulum model to resolve the conflicts between the sensed response predicted by the torsion-pendulum model and the perceptual response measured in experiments. The addition of adaptation results in the following transfer function:

$$\frac{\phi_c(s)}{\alpha(s)} = K\frac{\tau_a s}{(1+\tau_a s)}\frac{1}{(1+\tau_1 s)(1+\tau_2 s)}, \tag{18}$$

where τ_a is the adaptation time constant, and the gain K noted by Zacharias [12] is equal to $a\tau_1\tau_2$.

Zacharias [12] reported several experiments suggesting an additional lead component. With the addition of this component with time constant τ_L, a model representing both the semicircular canal dynamics and the neural transduction dynamics is now established:

$$\frac{\phi_c(s)}{\alpha(s)} = K\frac{\tau_a s}{(1+\tau_a s)}\frac{(1+\tau_L s)}{(1+\tau_1 s)(1+\tau_2 s)}, \tag{19}$$

Fernandez and Goldberg [17] determined average parameters for the semicircular canals of the squirrel monkey by direct measurement of the afferent nerves due to various angular acceleration inputs of different amplitudes and frequencies. Their transfer function relates the afferent firing rate of the vestibular nerve to the angular acceleration input:

$$\frac{AFR(s)}{\alpha(s)} = 3.44\frac{80s}{(1+80s)}\frac{(1+0.049s)}{(1+5.7s)(1+0.003s)}. \tag{20}$$

The model parameters were estimated with the exception of the short time constant, which was determined analytically based on the physiology of the endolymph.

Parameters for man are difficult to measure because direct measurement of the afferent nerve outputs of the vestibular system cannot be done and therefore most experiments were based on subjective responses or nystagmus tests. Several experiments reported by Zacharias [12] were performed to determine parameters of the torsion-pendulum model, with Young and Oman [16] also estimating the adaptation time constant. Zacharias [12] reported a value for τ_L of 0.06 seconds resulting from nystagmus tests.

From these results, a transfer function that can best relates the afferent response of the semicircular canals to the acceleration stimulus is proposed:

$$\frac{AFR(s)}{\alpha(s)} = 3.44 \frac{80s}{(1+80s)} \frac{(1+0.06s)}{(1+5.73s)(1+0.005s)}. \tag{21}$$

Otolith Model

Zacharias [12] reported that Meiry first investigated subjective responses to linear motion, obtaining a transfer function relating perceived velocity $\hat{v}$ to stimulus velocity v:

$$\frac{\hat{v}(s)}{v(s)} = \frac{K\tau_1 s}{(\tau_1 s+1)(\tau_2 s+1)}, \tag{22}$$

where τ_1 and τ_2 are otolith time constants, with $\tau_1 >> \tau_2$, and K is a gain term. Young and Meiry [18] noted that this model correctly predicted the phase of the perceived velocity and the time to detect motion under constant acceleration, but failed to predict the otoliths' response to sustained tilt angle as indicated by behavioral and physiological data. Young and Meiry then proposed the following revised model of specific force sensation that presumed the equivalence of both linear acceleration and tilt sensation:

$$\frac{\hat{f}(s)}{f(s)} = \frac{0.4(13.2s+1)}{(5.33s+1)(0.66s+1)}. \tag{23}$$

From the Young-Meiry model [18] and physiological knowledge of the otolith organ, Ormsby [19] estimated a model of the otolith afferent dynamics that neglected the short time constant:

$$\frac{AFR(s)}{f(s)} = 45\,\frac{10s+1}{5s+1}. \tag{24}$$

Fernandez and Goldberg [20] studied the discharge of otolith neurons in response to sinusoidal force variations in the squirrel monkey. Both regularly and irregularly discharging neurons were measured. Fernandez and Goldberg identified a ratio of

regular to irregular units to be approximately three to one. The frequency responses resulted in a transfer function of the form

$$H(s) = G_{DC}\frac{1+k_A\tau_A s}{1+\tau_A s}\frac{1+k_v(\tau_v s)^{k_v}}{1+\tau_M s} = G_{DC}\ H_A(s)\frac{H_v(s)}{H_M(s)}. \tag{25}$$

In Eqn. (25), the term H_v is a velocity-sensitive operator with a fractional exponent that provides most of the gain enhancement and phase lead found primarily in the irregular units. The value of k_v reflects the effectiveness of the lead operator and is closely related to the slope of the gain curve. The median parameters for both regular and irregular units for Eqn. (25) are given in Table 1 [20].

Table 1. Median Parameters for Regular and Irregular Units.

	k_v	k_A	τ_A	τ_M	G_{DC}
Regular	0.188	1.12	69 sec	16 msec	25.6 ips / g
Irregular	0.440	1.90	101 sec	9 msec	20.5 ips / g

Note that the gain terms for the Fernandez-Goldberg model are about one half of the gain value chosen by Ormsby. Due to the adaptation mechanism H_A in the Fernandez-Goldberg models, these gains would require a long duration step input to be realized in steady-state. Hosman [21] suggested a gain term of less magnitude than that used by Ormsby (G_{DC} = 33.3) that provides an improved approximation to the Fernandez-Goldberg responses.

Because of the fractional exponent in the transfer function of Eqn. (25), an elementary solution to its response cannot be readily obtained. However, an approximate solution to the response can be derived through the application of fractional calculus as described by Miller and Ross [22]. By using fractional calculus, the regular and irregular unit responses to a step input have been derived [23].

By using the long and lead time constants reported by Ormsby, selecting the short time constant from the Fernandez-Goldberg model, and including the gain suggested by Hosman, the following transfer function results for the afferent otolith dynamics [23]:

$$\frac{AFR(s)}{f(s)} = 33.3\frac{(10s+1)}{(5s+1)(0.016s+1)}. \tag{26}$$

INTEGRATED HUMAN PERCEPTION MODEL

Visually Induced Motion Sensation

The general characteristics of visually induced self-motion in the absence of confirming vestibular stimuli as reported by Young [24] and supported by other researchers is summarized. Young noted two distinct classes of visual cues for flight simulation: the foveal cues, the high acuity, high information-dense central field cues that

must be "read" to be interpreted, and the peripheral cues, the wide-field, lower acuity, rapidly moving cues that generate non-cognitive motion perception. These cues correspond respectively to the high static acuity, cone-filled fovea, and the high dynamic sensitivity, rod-filled periphery of the retina.

Brandt, et al. [25] demonstrated that the peripheral visual field is of primary importance in stimulating self-motion over the central visual field. Brandt, et al. [26] also demonstrated that background stimulation is dominant over foreground stimulation; movement in the background induces self-motion while if the foreground moved the stationary background inhibited circularvection. Held, et al. [27] showed that the spatial frequency of the visual scene also determines its effectiveness in generating self-motion. Young [24] commented that the peripheral visual field display should have a sufficient number of borders such as stars, clouds, or ground features to induce the perceived self-motion. Young also noted that the visual field velocity determines the magnitude of the self-motion up to a saturation velocity that most likely corresponds to the blurring of the visual field associated with increased visual acuity.

Young [24] found that the approximate frequency response for both circularvection and linearvection is flat from static inputs up to a frequency of 0.1 Hz, beyond which it decreases at least as rapidly as a first-order filter. Berthoz, et al. [28] confirmed these results for forward linearvection, with similar results obtained by Van der Steen [29] for yaw circularvection.

The latency of the onset of visually induced motion has an impact on motion perception in flight simulation. Several experimenters have quantified this phenomenon. Brandt, et al. [25] observed the latency to onset of circularvection to be about three to four seconds and independent of the stimulus magnitude. Howard and Howard [30] demonstrated that the latency is reduced with the presence of stationary objects in view and with fixation of the subject's gaze. With a stationary visual frame similar to the simulator cockpit video monitor and with fixation, they observed latencies of about 5 seconds that were relatively unchanged with stimuli from 5 to 25 deg/sec. Berthoz, et al. [28] observed latencies for linearvection of about 1 to 1.5 seconds for velocities measured between 0.2 and 1 m/sec.

Visual-Vestibular Interaction Model

Zacharias [31] reported that both psychophysical and neurophysiological studies support the theory that visual and vestibular cues are jointly processed to provide for a perceived sense of self-motion. Young [32] noted that visual motion cues dominate the perception of velocity in the steady state and at frequencies below 0.1 Hz. At higher frequencies, the vestibular cues will tend to dominate. Confirming vestibular cues, in the direction opposite to the visual field, can produce a rapid onset of the visual self-motion that is sustained by vision after the vestibular cues have been washed out. When visual and vestibular motion cues are in conflict, either due to the direction of motion or to a difference in magnitude, the vestibular cues will initially dominate. Young [32] first proposed that visual and vestibular cues are independently processed to produce two estimates of motion that are compared with one another to provide some measure of cue conflict.

Zacharias [31] developed a cue conflict model for yaw perception. For low conflict, i.e. when the cues are confirming, the perceived motion is calculated from a weighted sum of the two estimates. For high conflict, the weighting on the visual cue is reduced and that on the vestibular cue is increased until the conflict is reduced. Borah [33] later developed a visual-vestibular interaction model that involved the implementation of an optimal estimator as a "central processor" representation of sensory inputs that included a modified version of the cue conflict model proposed by Zacharias. Van der Steen [29] proposed a self-motion perception model in which vestibular and visual stimuli are combined to describe perceived self-motion. However, unlike the model proposed by Zacharias, cue conflict estimation is not considered.

Van der Steen [29] noted that psychophysical experiments concerning vection showed that the visual estimate of self-motion "attracts" the vestibular estimate of self-motion. This "visual attractor" component uses the visual and vestibular system's estimates of perceived self-motion. The difference between these cues is passed through a first-order low-pass filter H_{VA} with time constant τ_{VA} that represents the gradual build-up of self-velocity, forming the optokinetic influence:

$$H_{VA} = \frac{1}{1+\tau_{VA}s}. \tag{28}$$

A new visual-vestibular interaction model for rotational motion is proposed [34] and is shown in Figure 6. A second model for translational motion is also proposed with a similar structure that incorporates a model of the otolith dynamics [34].

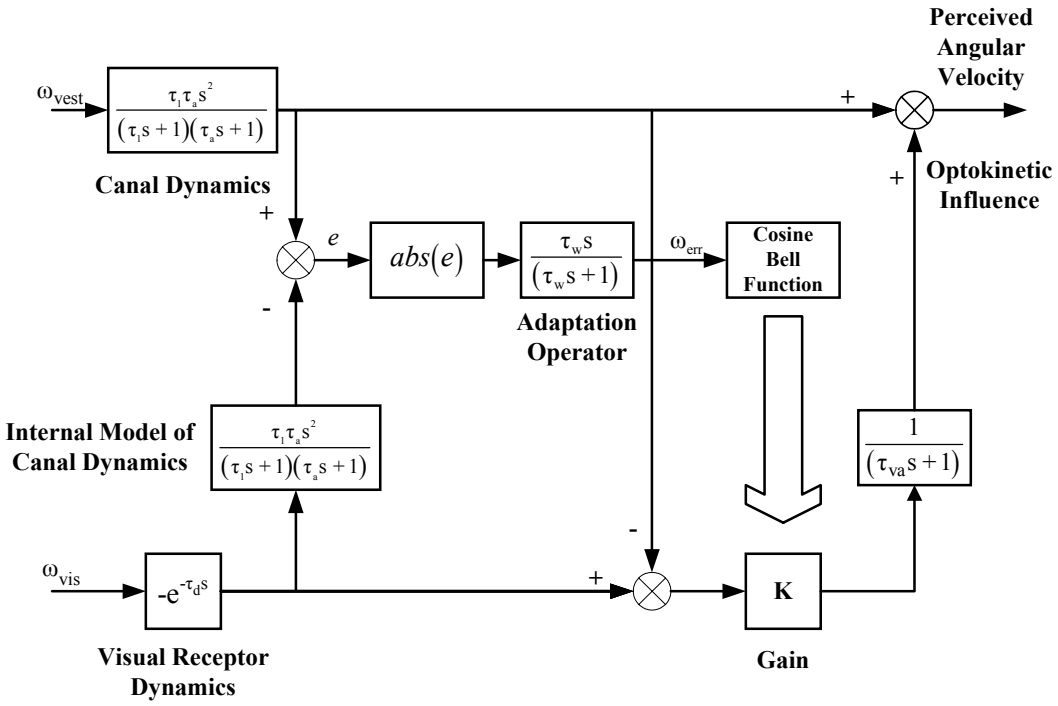

Figure 6. Proposed Visual-Vestibular Model for Rotational Motion.

Using a concept suggested by Van der Steen [29], the vestibular model consists of the afferent dynamics cascaded with a neural filter gain, resulting in a perceived response to vestibular stimuli. The optokinetic influence proposed by Van der Steen is also implemented. The time constant τ_{VA} governing the optokinetic influence is chosen to be 1.592 seconds, which is equal to the 0.1 Hz low-pass filter break frequency noted by Young [24].

As proposed by Zacharias [31], the visual cue is passed through an internal model of the vestibular dynamics to produce an "expected" vestibular signal that is then subtracted from the actual vestibular signal. To allow for long-term resolution of steady state conflict the absolute value of this error is passed through an adaptation operator to generate a conflict signal ω_{err}. The adaptation operator determines how long a steady state inter-cue conflict should be allowed to continue by washing out the conflict signal.

From ω_{err} the weighting of the optokinetic gain K is then computed by a modified cosine bell function suggested by Borah [33]. The gain K varies between zero and one. A large conflict signal greater than the conflict threshold ε will drive the visual gain to zero, whereas a small signal below the threshold value will drive the gain to a value between zero and one, approaching one as ω_{err} approaches zero. For $\omega_{err} < 0$, the gain remains at one. As proposed by Borah [33] the vestibular path gain remains fixed at unity. The conflict threshold ε is chosen to equal the vestibular indifference motion threshold. A time constant $\tau_w = 8$ seconds is chosen to produce the latency responses noted in the literature.

NONLINEAR MOTION CUEING ALGORITHM

Algorithm Formulation

This approach has been suggested by Ish-Shalom [35], and Cardullo and Kosut [36] have proposed the algorithm structure. The structure of the problem is illustrated in Figure 7.

The system equation is developed by the same technique shown for the linear optimal algorithm. The parameters for the revised semicircular canals and otolith models (Eqns. (21) and (26) respectively) will be used, and the confirming case of the integrated perceptual model (with the optokinetic gain fixed at unity) will also be incorporated into each perceptual channel. The system equation and cost function are then transformed to the standard form of Eqn. (10). The cost function is then augmented with an additional term $e^{2\alpha t}$ proposed by Anderson and Moore [37]:

$$J' = E\left\{\int_{t_0}^{t_1} e^{2\alpha t}\left(\mathbf{x}^{\mathbf{T}}\mathbf{R}_{\mathbf{1}}'\mathbf{x} + \mathbf{u}'^{\mathbf{T}}\mathbf{R}_{\mathbf{2}}\mathbf{u}'\right)dt\right\}, \tag{29}$$

where $\mathbf{R}_{\mathbf{1}}'$ is positive definite, $\mathbf{R}_{\mathbf{2}}$ is positive semi-definite, and the scalar coefficient α represents a minimum degree of stability in the closed-loop system where $\alpha > 0$.

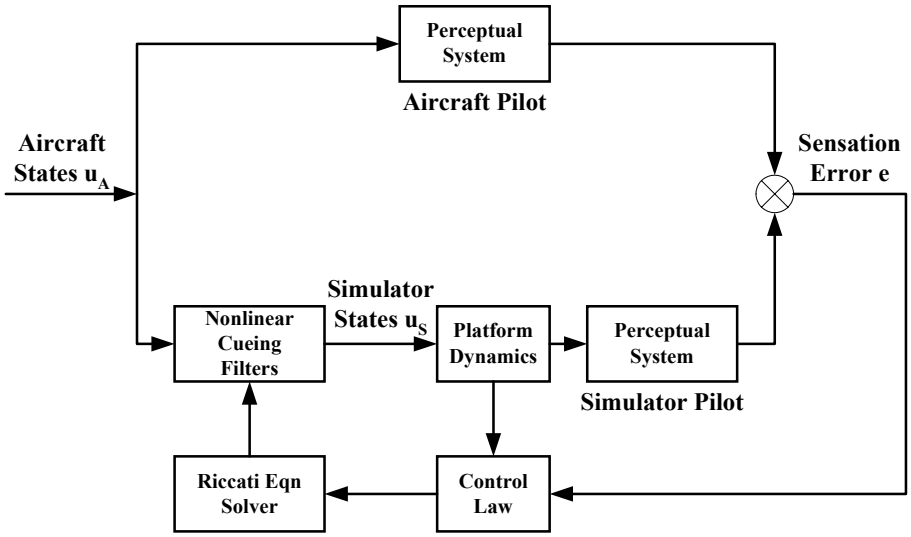

Figure 7. Problem Structure for Nonlinear Optimal Cueing Algorithm.

Anderson and Moore [37] show that the system equation and cost function can be transformed to eliminate the exponential term, resulting in

$$\begin{aligned} \dot{\tilde{\mathbf{x}}} &= \left(\mathbf{A}' + \alpha\mathbf{I}\right)\tilde{\mathbf{x}} + \mathbf{B}\tilde{\mathbf{u}} + \mathbf{H}'\mathbf{w}\,, \\ \tilde{J}' &= E\left\{\int_{t_0}^{t_1}\left(\tilde{\mathbf{x}}^{\mathrm{T}}\mathbf{R}_1'\tilde{\mathbf{x}} + \tilde{\mathbf{u}}^{\mathrm{T}}\mathbf{R}_2\tilde{\mathbf{u}}\right)dt\right\}, \end{aligned} \tag{30}$$

where $\tilde{\mathbf{x}} = e^{\alpha t}\mathbf{x}$, $\tilde{\mathbf{u}} = e^{\alpha t}\mathbf{u}'$, and $\mathbf{H}' = \mathbf{H}e^{\alpha t}$. We now wish to compute the simulator control input $\mathbf{u}_S$ that minimizes the cost function given in Eqn. (31). For this problem, $\mathbf{A}' + \alpha\mathbf{I}$ is positive definite, $\left(\mathbf{A}' + \alpha\mathbf{I}, \mathbf{B}\right)$ is controllable and $\left(\mathbf{A}' + \alpha\mathbf{I}, \mathbf{R}_1'\right)$ is observable. Under these conditions, the cost function is minimized when

$$\mathbf{u}_S = -\mathbf{K}(\alpha)\mathbf{x}\,, \tag{31}$$

where $\mathbf{K}(\alpha) = \mathbf{R}_2^{-1}\left(\mathbf{B}^{\mathrm{T}}\mathbf{P}(\alpha) + \mathbf{R}_{12}\right)$, and $\mathbf{P}(\alpha)$ is the solution of the algebraic Riccati equation

$$\left(\mathbf{A}' + \alpha\mathbf{I}\right)\mathbf{P}(\alpha) + \mathbf{P}(\alpha)\left(\mathbf{A}' + \alpha\mathbf{I}\right) - \mathbf{P}(\alpha)\mathbf{B}\mathbf{R}_2^{-1}\mathbf{B}^{\mathrm{T}}\mathbf{P}(\alpha) + \mathbf{R}_1' = \mathbf{0}\,. \tag{32}$$

Anderson and Moore note that for $\alpha > 0$, the resulting closed-loop system

$$\dot{\mathbf{x}} = \left[\mathbf{A}' - \mathbf{B}\mathbf{K}(\alpha)\right]\mathbf{x} \tag{33}$$

is asymptotically stable, with the property that all the eigenvalues lie to the left of -α, i.e. the degree of stability of the closed-loop system is at least α. A nonlinear control law is chosen to make α dependent upon the system states:

$$\alpha = \mathbf{e}^T\mathbf{Q}_1\mathbf{e} + \mathbf{x}_d^T\mathbf{Q}_2\mathbf{x}_d \,, \tag{34}$$

where $\mathbf{Q}_1$ and $\mathbf{Q}_2$ are weighting matrices and are at least positive semi-definite. As the system states increase in magnitude, i.e. large perceptual errors and platform motions, then α increases, resulting in faster control action and increased system stability. For small state magnitudes there will be limited control action. The actual nonlinear control law is then determined by solving the Riccati equation of Eqn. (32) in real time as a function of α.

Real Time Solution of the Riccati Equation

Solving the nonlinear Riccati equation in real time is a computational challenge as a new solution is required at each time step. Since the solution to the preceding time step is available, it is advantageous to use this as an initial solution when computing the solution for the current time step, thus reducing the computational burden. The initial Riccati equation solution to the linear optimal algorithm that is computed off-line in MATLAB is available and can be used as the initial solution for the first time step. To this end we desire a technique that assumes the initial solution is "close" to the final solution at a given time step.

Three techniques have been evaluated for implementation. Blackburn [38] developed a method of solution by using a Newton-Raphson iteration. With this technique, computation of the Jacobian matrix as a Kronecker product is required along with matrix inversion, which can result in a singular solution for an ill-conditioned system. Neurocomputing approaches suggested by Wang and Wu [39] and Ham and Collins [40] eliminate both operations, thus reducing the real time computational burden. For these reasons, the neurocomputing approaches are further evaluated. The neurocomputing approach proposed by Ham and Collins [40] uses a structured neural network for obtaining the Riccati equation computational solution **V** as shown in Figure 8.

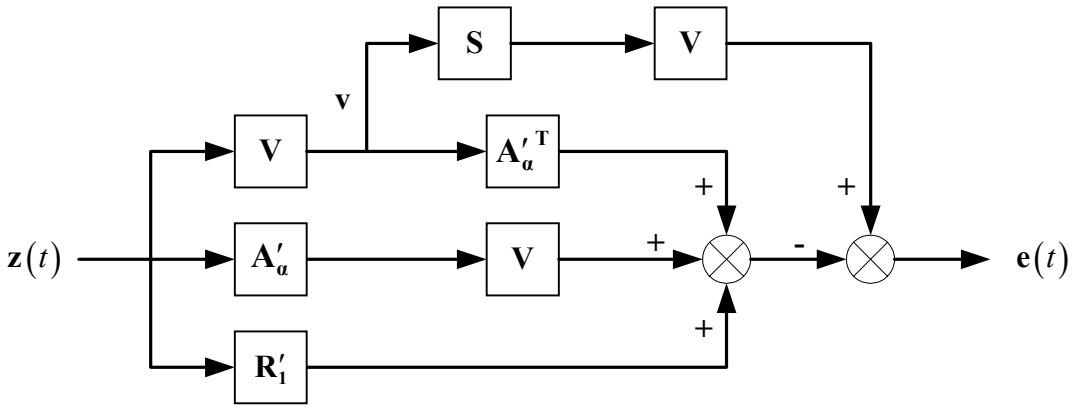

Figure 8. Structured Neural Network for Solving the Riccati Equation.

The error signal $\mathbf{e}(t)$ in Figure 8 is given as

$$\mathbf{e}(t) = \left[\mathbf{V}(t)\mathbf{S}\mathbf{V}(t) - \mathbf{A}_{\alpha}'^{\mathrm{T}}\mathbf{V}(t) - \mathbf{V}(t)\mathbf{A}_{\alpha}' - \mathbf{R}_1' \right]\mathbf{z}(t), \tag{35}$$

where $\mathbf{S} = \mathbf{B}\mathbf{R}_2^{-1}\mathbf{B}$, $\mathbf{A}_{\alpha}' = \mathbf{A}' + \alpha\mathbf{I}$, and $\mathbf{z}(t)$ is an excitatory input signal. An energy function is then formulated as $\mathbf{E}(\mathbf{V}) = \frac{1}{2}\|\mathbf{e}\|_2^2$ (where $\|\bullet\|_2$ is the Euclidean norm), which is minimized using the method of steepest descent, resulting in a system of first-order matrix differential equations

$$\begin{aligned} \dot{\mathbf{V}}(t) = \frac{\mu}{2}\big[& \mathbf{A}_{\alpha}'\,\mathbf{e}(t)\mathbf{z}^{\mathrm{T}}(t) + \mathbf{z}(t)\mathbf{e}^{\mathrm{T}}(t)\mathbf{A}_{\alpha}'^{\mathrm{T}} + \mathbf{e}(t)\mathbf{z}^{\mathrm{T}}(t)\mathbf{A}_{\alpha}'^{\mathrm{T}} \\ & + \mathbf{A}_{\alpha}'\mathbf{z}(t)\mathbf{e}^{\mathrm{T}}(t) - \mathbf{e}(t)\mathbf{v}^{\mathrm{T}}(t)\mathbf{S} - \mathbf{S}\mathbf{v}(t)\mathbf{e}^{\mathrm{T}}(t)\big], \end{aligned} \tag{36}$$

where $\mu > 0$ is the learning rate parameter, and $\mathbf{v}(t) = \mathbf{V}(t)\mathbf{z}(t)$ as shown in Figure 8. Ham and Collins [40] note that the external excitatory vector input signals $z(t)$ are a set of linearly independent bi-polar vectors given as

$$z^{(1)} = \begin{bmatrix} 1 & -1 & \cdots & -1 \end{bmatrix}, z^{(2)} = \begin{bmatrix} -1 & 1 & \cdots & -1 \end{bmatrix}, z^{(n)} = \begin{bmatrix} -1 & -1 & \cdots & 1 \end{bmatrix}, \tag{37}$$

where each vector is presented once to the neural network in an iteration, i.e. for one iteration there is a total of n presentations of the bi-polar input vectors.

Nonlinear Algorithm Evaluation

Responses using the neurocomputing approach suggested by Ham and Collins [40] are examined. The yaw mode responses for an angular acceleration doublet of 0.1 rad/s^2 magnitude and 5-second duration are shown in Figure 9. A learning rate parameter $\mu = 10^{-4}$ is used in computing the solution to the Riccati equation. Note that the negative angular velocity cue is reduced with the nonlinear algorithm. The displacement command shows an increased peak magnitude along with a reduced overshoot. The command returns to the neutral state (zero displacement) in the same time as the response from the linear algorithm, while the response with the neurocomputing solver of Wang and Wu [39] requires more time to return to the neutral state.

For the heave mode based upon the integrated perception model, the off-line solution to the Riccati equation initially produced one closed-loop eigenvalue of zero, which results in the linear algorithm being very difficult to tune off-line. This eigenvalue is a result of including the optokinetic channel in the algorithm formulation; the formulation based on the vestibular model alone does not produce a zero eigenvalue. A state reduction using the MATLAB function **"minreal"** was performed on the perceptual model, removing one state and in turn eliminating the closed-loop eigenvalue of zero.

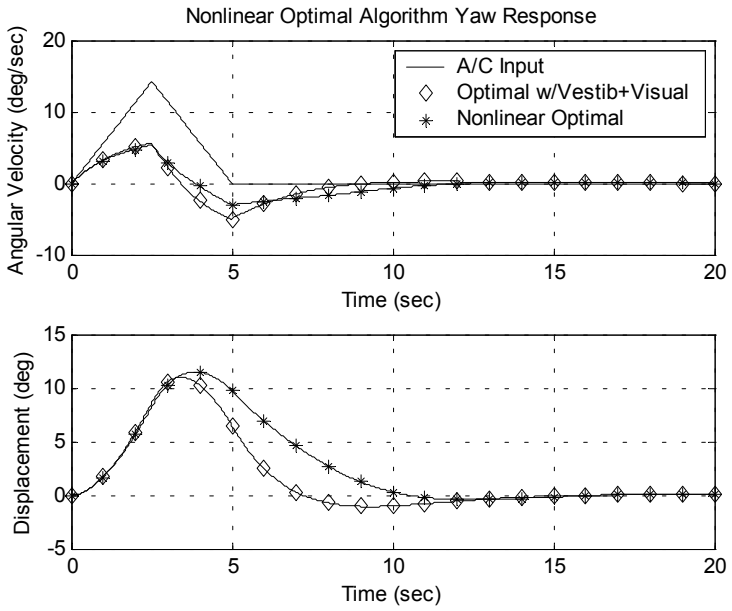

Figure 9. Nonlinear Algorithm Yaw Mode Responses with Riccati Equation Neurocomputing Solver.

The heave mode responses for a square pulse input of 1 m/s^2 and 10-second duration are shown in Figure 10. A learning rate parameter $\mu = 6 \times 10^{-5}$ is used in computing the solution to the Riccati equation. The onset cue is sustained, with the negative cue at the end of the pulse reduced in magnitude as compared to the linear algorithm response. The displacement command shows a reduction in the peak displacement that can be used to advantage when scaling the response within the motion platform limits, i.e. a larger percentage of the onset cue will remain as compared to the linear case. In this mode an upper limit of 0.12 is placed on α that will affect the magnitude of the sustained response for large magnitude inputs; an increase in this value results in a false cue at the end of the pulse along with a distorted response. The response with the neurocomputing solver of Wang and Wu [39] generated a very small difference from the linear response.

The systems of first-order differential equations given for the neurocomputing solver in Eqn. (37) require a numerical integration algorithm. A series of algorithms (Euler, 2nd-order Adams-Bashforth, 2nd- and 4th-order Runge-Kutta) have been evaluated for each neurocomputing solver. No improvement was noticed with the higher-order methods as compared to the Euler method for either algorithm.

The responses using the neurocomputing solver proposed by Wang and Wu [39] are sensitive to the magnitude and stiffness of the closed-loop eigenvalues, with the responses dependent upon the choice and structure of the activation functions. The approach proposed by Ham and Collins [40] utilizes a structured network without activation functions; the responses are more robust with respect to the closed-loop eigenvalues. This solver also yields improved responses and convergence with less computational burden; only one solver iteration was required per time step. For these

reasons the neurocomputing solver proposed by Ham and Collins is chosen for implementation in the motion system.

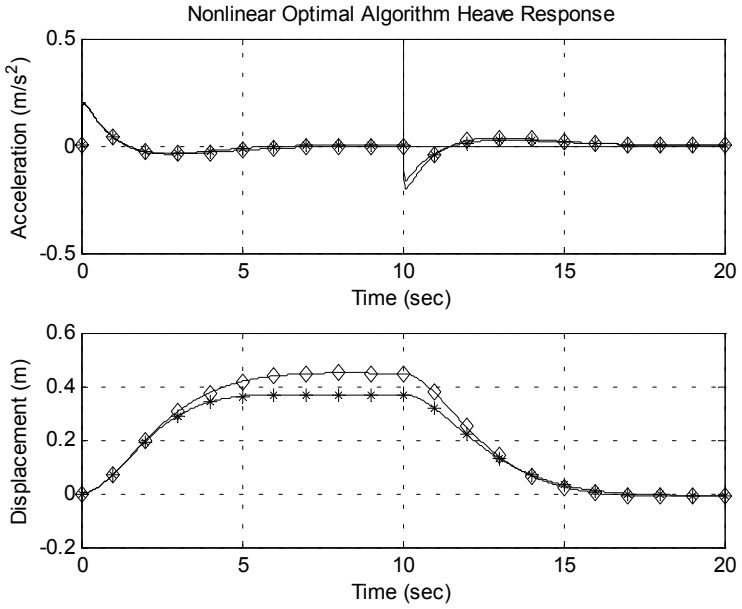

Figure 10. Nonlinear Algorithm Heave Mode Responses with Riccati Equation Neurocomputing Solver.

A model of the nonlinear algorithm has been developed for the two-degree-of-freedom longitudinal mode. The initial formulation with the integrated perception model resulted in a higher-order system (13^{th}-order) that is much larger than either yaw or heave (5^{th}-order). Two closed-loop eigenvalues of zero resulted from the linear algorithm solution. The first originated from the platform state θ noted in Eqn. (14). The second resulted from the optokinetic channel for the translational degree-of-freedom. Removal of the additional platform state combined with a state reduction of the perceptual model eliminates the two closed-loop eigenvalues of zero, reducing the system to 11^{th}-order.

Figure 11 compares the linear algorithm response based upon the integrated perceptual model to the response based upon the vestibular models only. A ramp to step surge input of 0.5 m/s^2 and slope 3 $m/s^2/s$ is applied to both models. Note that the specific force response with the perceptual model increases to the aircraft input after onset and does not wash out as a function of time, resulting from the steady-state tilt angle sustaining a constant magnitude. A decrease in the pitch angular velocity or tilt rate is also observed along with a reduction in the negative peak to about 0.5 deg/sec.

Application of the nonlinear algorithm does not change the specific force response as compared to the linear algorithm. An increase in the simulator angular velocity command is observed, with a faster return to zero magnitude. This results in an increase in the peak tilt angle, with the response settling faster to the steady-state tilt angle. A small reduction in the simulator displacement also results. The benefit of these changes needs to be further investigated combined with the application of nonlinear scaling in producing actuator extensions within the motion platform limits.

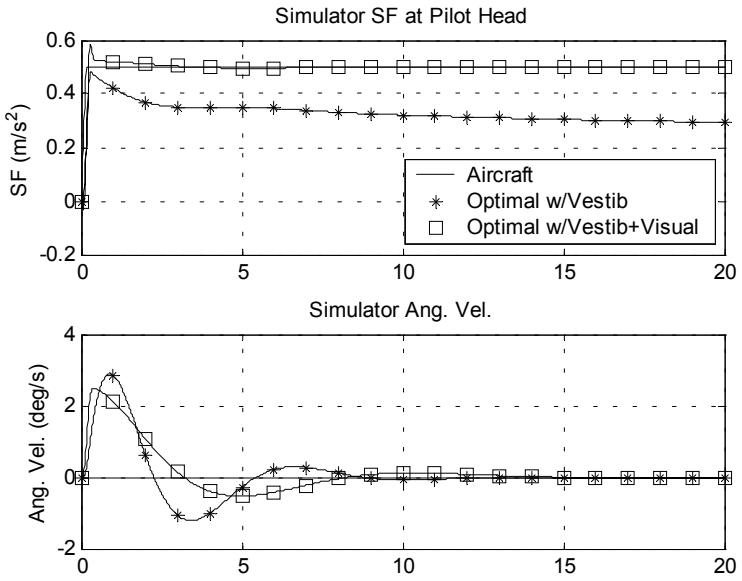

Figure 11. Surge and Tilt Coordination Commands for Perceptual-Based Linear Algorithm.

Comparisons of degree-of-freedom commands will be made between the proposed algorithm and the adaptive algorithm. Nonlinear scaling parameters will be implemented for the nonlinear algorithm to optimize performance within the actuator extension limits of the motion system. Algorithm degree-of-freedom and actuator extension commands will be computed for test runs for each algorithm in the longitudinal, lateral, yaw, and heave modes. Comparisons will be made of specific force at the pilot's head and platform angular velocity, as well as responses filtered through the modified vestibular system models and the integrated perception model.

CUEING ALGORITHM PILOTED PERFORMANCE TESTING

The effectiveness of the nonlinear algorithm as compared to the adaptive and linear optimal algorithms will be assessed in piloted simulations. Testing will be conducted on two motion systems at the NASA Langley Research Center: the Visual Motion Simulator (VMS) and the Cockpit Motion Facility (CMF). Preliminary testing is currently being performed on the VMS with the adaptive and linear optimal algorithms. As a result of these preliminary tests the nonlinear scaling coefficients will be adjusted for each mode. Final testing and evaluation will be conducted on the CMF with the nonlinear algorithm.

A group of pilots will execute a set of maneuvers on the CMF. For each maneuver the simulated aircraft dynamics is generated from manual pilot control. The pilot control inputs (throttle, elevator, aileron, and rudder) will be sampled for each maneuver. Accelerometer measurements for specific force and angular acceleration at the platform motion-base centroid in six degrees of freedom will be recorded for each maneuver.

Pilot perception (as computed from the proposed vestibular models and the integrated perception model) will be recorded for each maneuver. From the pilot control inputs,

power spectral density, crossover frequency, and phase angle will be analyzed to determine the effect of motion platform response upon pilot performance. The pilot will also evaluate each maneuver subjectively, using the Cooper-Harper rating scale as a metric. From these data, the fidelity of each algorithm will be benchmarked in replicating pilot performance and workload of actual aircraft maneuvers.

SUMMARY

An improved linear optimal algorithm based upon angular velocity input was developed. Cueing responses to a surge input show this algorithm has improved tracking capability without a false cue and a lower tilt rate at onset, while producing a lower magnitude specific force response as compared to the adaptive algorithm.

Literature studies of the human vestibular system led to mathematical models of the semicircular canal and otolith organs with revised parameters. An integrated model of human motion perception was proposed that includes the vestibular models and incorporates the nonlinear interaction between the vestibular and visual stimuli. The addition of the optokinetic influence in the linear algorithm was shown to improve the response to a surge input, producing a specific force response with no steady-state washout and a further decrease in the tilt rate.

A nonlinear cueing algorithm was developed that combines features of the adaptive and optimal algorithms, and incorporates the vestibular and integrated perception models. A nonlinear control law was proposed that requires the solution of the Riccati equation in real time. A neurocomputing approach has been implemented for this task. Results for the yaw mode reveal that the nonlinear algorithm improves the motion cues by reducing the magnitude of negative cues. The heave mode responses show a reduction in the peak onset displacement command that, when scaling the response within the motion platform limits, will yield an increased onset cue. The neurocomputing solver will yield responses that are robust with respect to the closed-loop eigenvalues, with less computational burden as compared to a second neurocomputing solver.

Further investigation is needed to assess the improvements resulting from the nonlinear algorithm for two-degree-of-freedom longitudinal and lateral modes. Comparisons of algorithm responses, as well as responses from the vestibular and integrated perception models will then be made with the adaptive algorithm. The performance of the new algorithm will then be demonstrated in piloted simulations on the cockpit motion facility (CMF) at the NASA Langley Research Center.

ACKNOWLEDGEMENTS

This research was supported for the past year by a Link Foundation Fellowship, and has also been supported by the NASA Langley Research Center in Hampton, Virginia. Both means of support are gratefully acknowledged. The work presented in this paper formed the basis for my dissertation prospectus presented earlier this summer.

REFERENCES

[1] A. J. Gundry, *Thresholds to Roll Motion in a Flight Simulator.* Journal of Aircraft, 14(7): p. 624-631 (1977).

[2] S. L. Buckingham, *Helicopter Flight Research - A Demanding Application of Piloted Simulation*. in *International Conference on Flight Simulation of Helicopters, Proceedings of the Royal Aeronautical Society,* London (1985).

[3] J. L. Meiry, *The Vestibular System and Human Dynamic Space Orientation*. Sc.D. Thesis, Massachusetts Institute of Technology: Cambridge, MA (1965).

[4] J. R. Hall, *Motion Versus Visual Cues in Piloted Flight Simulation*. in *AGARD Conference Proceedings No. 249, Piloted Aircraft Environment Simulation Techniques,* Brussels, Belgium (1978).

[5] W. Wu and F. M. Cardullo, *Is There an Optimum Cueing Algorithm?* in *AIAA Modeling and Simulation Technologies Conference*, New Orleans, LA (1997).

[6] R. V. Parrish, J. E. Dieudonne, and D. J. Martin, Jr., *Motion Software for a Synergistic Six-Degree-of-Freedom Motion Base.* NASA TND-7350 (1973).

[7] R. Sivan, J. Ish-shalom, and J. K. Huang, *An Optimal Control Approach to the Design of Moving Flight Simulators.* IEEE Transactions on Systems, Man, and Cybernetics, 12(6): p. 818-827 (1982).

[8] L. D. Reid and M. A. Nahon, *Flight Simulation Motion-base Drive Algorithms: Part 1 - Developing and Testing the Equations*. UTIAS Report No. 296, CN ISSN 0082-5255 (1985).

[9] W. Wu, *Development of Cueing Algorithm for the Control of Simulator Motion Systems*. M.S. Thesis, State University of New York at Binghamton: Binghamton, NY (1997).

[10] H. Kwakernaak and R. Sivan, *Linear Optimal Control Systems*. John Wiley and Sons, Inc., New York (1972).

[11] R. J. Telban, F. M. Cardullo, and J. A. Houck, *Developments in Human Centered Cueing Algorithms for Control of Flight Simulator Motion Systems*. in *AIAA Modeling and Simulation Technologies Conference*, Portland. OR (1999).

[12] G. L. Zacharias, *Motion Cue Models for Pilot-Vehicle Analysis*. Department of Defense Report AMRL-TR-78-2 (1978).

[13] A. A. Van Egmond, J. J. Groen, and L. B. W. Jongkees, *The Mechanics of the Semicircular Canal.* Journal of Physiology, 110: p. 1-17 (1949).

[14] R. A. Mayne, *A Systems Concept of the Vestibular Organs*, in *Handbook of Sensory Physiology, Vestibular System*, H. H. Kornhuber, Editor. Springer-Verlag, New York. p. 493-560 (1974).

[15] R. Schmid, A. Buizza, and D. Zambarbieri, *Modelling of the Vestibulo-Ocular Reflex and its Use in Clinical Vestibular Analysis*, in *Applied Physiological Mechanics*. OPA, Amsterdam, B.V. p. 779-893 (1979).

[16] L. R. Young and C. M. Oman, *Model for Vestibular Adaptation to Horizontal Rotation.* Aerospace Medicine, 40(10): p. 1076-1080 (1969).

[17] C. Fernandez and J. M. Goldberg, *Physiology of Peripheral Neurons Innervating Semicircular Canals of the Squirrel Monkey. II. Response to Sinusoidal Stimulation and Dynamics of Peripheral Vestibular System.* Journal of Neurophysiology, 34(4): p. 661-675 (1971).

[18] L. R. Young and J. L. Meiry, *A Revised Dynamic Otolith Model.* Aerospace Medicine, 39(6): p. 606-608 (1968).
[19] C. C. Ormsby, *Model of Human Dynamic Orientation*. Ph.D. Thesis, Massachusetts Institute of Technology: Cambridge, MA (1974).
[20] C. Fernandez and J. M. Goldberg, *Physiology of Peripheral Neurons Innervating Otolith Organs of the Squirrel Monkey, I. Response to Static Tilts and to Long-Duration Centrifugal Force.* Journal of Neurophysiology, 39(5): p. 970-983 (1976).
[21] R. J. Hosman, *Pilot's Perception and Control of Aircraft Motions*. Ph.D. Thesis, Delft University of Technology: Delft, The Netherlands (1996).
[22] K. S. Miller and B. Ross, *An Introduction to the Fractional Calculus and Fractional Differential Equations*. John Wiley and Sons, Inc., New York (1993).
[23] R. J. Telban, F. M. Cardullo, and L. Guo, *Investigation of Mathematical Models of Otolith Organs for Human Centered Motion Cueing Algorithms*. in *AIAA Modeling and Simulation Technologies Conference*. Denver, CO (2000).
[24] L. R. Young, *Visually Induced Motion in Flight Simulation*. in *AGARD Symposium on Flight Simulation*, Brussels, Belgium (1978).
[25] T. Brandt, J. Dichgans, and E. Koenig, *Differential Aspects of Central Versus Peripheral Vision on Egocentric and Exocentric Perception.* Experimental Brain Research, 16(476-491) (1973).
[26] T. Brandt, E. R. Wist, and J. Dichgans, *Foreground and Background in Dynamic Spatial Orientation.* Perception & Psychophysics, 17(5): p. 497-503 (1975).
[27] R. Held, J. Dichgans, and J. Bauer, *Characteristics of Moving Visual Scenes Influencing Spatial Orientation.* Vision Research, 15: p. 357-365 (1975).
[28] A. Berthoz, B. Pavard, and L. R. Young, *Perception of Linear Horzontal Self-Motion Induced by Peripheral Vision (Linearvection).* Experimental Brain Research, 23: p. 471-489 (1975).
[29] H. Van der Steen, *Self-Motion Perception*. Ph.D. Thesis, Delft University of Technology: Delft, The Netherlands (1998).
[30] I. P. Howard and A. Howard, *Vection: The Contributions of Absolute and Relative Motion.* Perception, 23: p. 745-751 (1994).
[31] G. L. Zacharias, *Motion Sensation Dependence on Visual and Vestibular Cues*. Ph.D. Thesis, Massachusetts Institute of Technology: Cambridge, MA (1977).
[32] L. R. Young, *On Visual-Vestibular Interaction*. in *Fifth Symposium on the Role of the Vestibular Organs in Space Exploration*, Pensacola, FL (1970).
[33] J. Borah, L. R. Young, and R. E. Curry, *Optimal Estimator Model for Human Spatial Orientation: Representation of Three-Dimensional Space in the Vestibular, Ocolumotor, and Visual Systems*, in *The New York Academy of Sciences*. New York, New York. p. 51-73 (1988).
[34] R. J. Telban and F. M. Cardullo, *An Integrated Model of Human Motion Perception with Visual-Vestibular Interaction*. in *AIAA Modeling and Simulation Technologies Conference,* Montreal, Canada (2001).
[35] J. Ish-Shalom, *Design of Optimal Motion for Flight Simulators*. Ph. D. Thesis, Massachusetts Institute of Technology: Cambridge, MA (1982).
[36] F. M. Cardullo and R. L. Kosut, *Old Problem/New Solutions: Motion Cuing Problems Revisited*. in *AIAA Flight Simulation Technologies Conference*, Niagara Falls. NY (1983).

[37] B. D. Anderson and J. B. Moore, *Linear Optimal Control*. 1971: Prentice-Hall, Inc., Englewood Cliffs, NJ (1971).
[38] T. R. Blackburn, *Solution of the Algrebraic Riccati Equation via Newton-Raphsen Iteration.* AIAA Journal, 6(5): p. 951-953 (1969).
[39] J. Wang and G. Wu, *A Multilayer Recurrent Neural Network for Solving Continuous-Time Algebraic Riccati Equations.* Neural Networks, 11: p. 939-950 (1998)
[40] F. M. Ham and E. G. Collins, *A Neurocomputing Approach for Solving the Algebraic Matrix Riccati Equation*. in *IEEE International Conference on Neural Networks* (1996).